JOURNAL OF COMPUTATIONAL PHYSICS 99, 288–298 (1992)

How to Discretize the Pressure Gradient for Curvilinear MAC Grids

ROBERT S. BERNARD

US Army Engineer Waterways Experiment Station, 3909 Halls Ferry Road, Vicksburg, Mississippi 39180

AND

HARTMUT KAPITZA

Forschungszentrum Geesthacht, Postfach 1160, 2054 Geesthacht, Germany

Received April 27, 1990; revised April 12, 1991

Curvilinear coordinates present certain difficulties for incompressible flow calculations with marker-and-cell (MAC) grids. Among these are questions regarding the discretization of derivatives in the pressure gradient, which should remain irrotational while maintaining conservation of mass. This paper examines alternative approximations for pressure derivatives next to the boundaries and for coordinate derivatives throughout the flow. Several combinations of alternatives are tested for their ability to remove continuity violations, without adding vorticity, in channels that have been fitted with nonorthogonal MAC grids. Each of these combinations achieves conservation of mass, but only one of them makes the pressure gradient effectively irrotational. The latter condition is achieved by using identical approximations for coordinate derivatives and pressure derivatives throughout the flow, and by using one-sided approximations next to the boundaries for ambiguous derivatives in the off-boundary direction.

1. INTRODUCTION

A marker-and-cell (MAC) grid is an array of discrete cells with spatial coordinates defined at the cell corners, pressure at the cell centers, and velocity on the cell faces. Since their introduction by Harlow and Welch [3], MAC grids have been widely used for incompressible flow [2, 6–8], because they facilitate the discretization of the continuity equation for conservation of mass. In numerical models for atmospheric flow, these grids are also known as Arakawa-C grids [5].

When MAC grids are used with general curvilinear coordinates, ambiguities arise due to the staggered locations of different variables, and special care is needed in the treatment of terms arising from nonuniformity and nonorthogonality of the grid. This is particularly true with the pressure gradient, which ideally should be irrotational and should add no vorticity to the flow.

In this paper we investigate the discretization of the pressure gradient for incompressible flow on curvilinear MAC grids, with emphasis on pressure derivatives next to boundaries, and coordinate derivatives throughout the flow. Thus, we consider a divergence-free velocity $\mathbf{u}$ and another velocity $\mathbf{u}'$, related by

$$\mathbf{u} = \mathbf{u}' - \rho^{-1} \nabla \phi \tag{1.1}$$

such that

$$\nabla \cdot \mathbf{u} = 0 \tag{1.2}$$

and

$$\nabla^2 \phi = \rho \nabla \cdot \mathbf{u}', \tag{1.3}$$

where ∇ is the gradient operator, ϕ is a scalar potential, ρ is density, and boldface type denotes vectors.

Starting with a divergence-free velocity at time t and enforcing Eq. (1.2) thereafter, let $\mathbf{u}$ be the velocity obtained by time-integrating the incompressible Euler or Navier–Stokes equations from t to $t + \Delta t$. If $\mathbf{u}'$ is the velocity obtained by doing the same integration *without* a pressure gradient, then

$$\phi = \int_t^{t+\Delta t} p \, dt', \tag{1.4}$$

where p is pressure. If p is construed to be the *average* pressure during the interval Δt, then Eq. (1.4) reduces to

$$\phi = p \, \Delta t. \tag{1.5}$$

0021-9991/92 $3.00

In this context the scalar potential is proportional to the average pressure in a given time interval, and it plays the same role in Eq. (1.1) as the pressure does in the incompressible Euler and Navier–Stokes equations. Specifically, it must eliminate any contribution to the velocity that violates Eq. (1.2), but it should add no vorticity to the flow. If one knows how to discretize $\nabla\phi$ so that this is accomplished for Eq. (1.1), then one also knows how to discretize ∇p for incompressible flow.

In the sections that follow, we develop discrete analogs for Eqs. (1.1)–(1.3) in two-dimensional curvilinear coordinates. Using uniform and nonuniform MAC grids for uniform flow in a straight channel, we then examine the effect of $\nabla\phi$ upon $\mathbf{u}$ when $\mathbf{u}'$ is vorticity-free but not divergence-free. The streamlines for the computed flow should be perfectly straight in all the test calculations. For nonuniform, nonorthogonal grids, however, the flow is noticeably distorted by the discrete gradient unless (a) identical approximations are used for coordinate derivatives and pressure derivatives throughout the flow, and (b) one-sided approximations are used next to the boundaries for ambiguous derivatives in the off-boundary direction. Each of these measures is necessary to keep the pressure gradient from creating spurious vorticity on general curvilinear MAC grids.

Throughout this paper the discretization problem will be considered only in two dimensions. The extension to three dimensions is straightforward, but it offers no additional insight concerning the discretization of the pressure gradient.

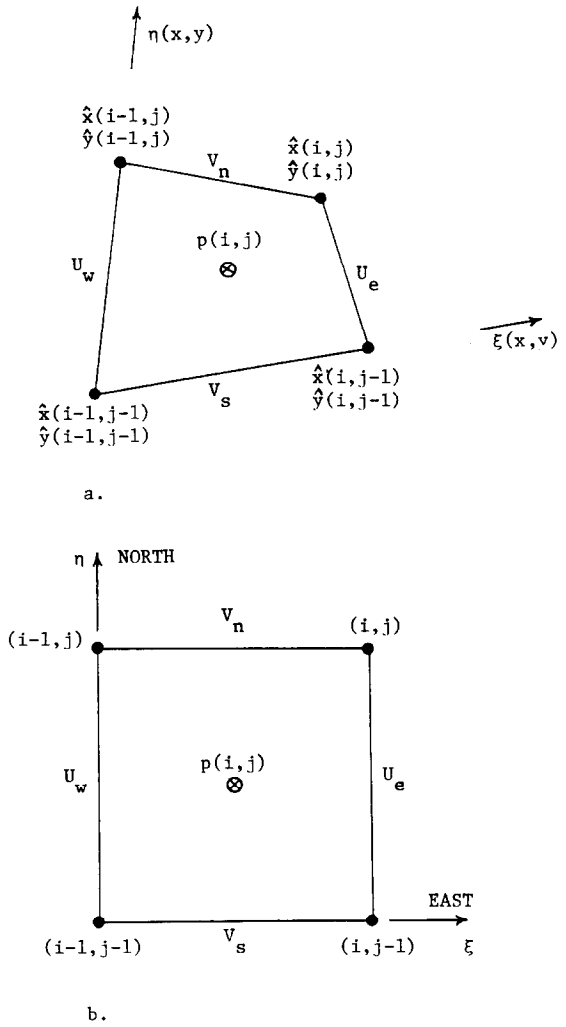

FIG. 1. Orientation of MAC grid cell in (a) cartesian (x, y) and (b) computational (ξ, η) planes.

2. CURVILINEAR COORDINATES

Let (ξ, η) be the curvilinear coordinates, and let the computational grid have unit spacing $(\Delta\xi = \Delta\eta = 1)$ in the computational (ξ, η) plane, so that integers (i, j) can be used for the discrete curvilinear coordinates. Integers can be used for (ξ, η) because the coordinate transformation determines the grid spacing in the cartesian plane, and the choice of spacing in the computational plane is arbitrary [10]. Figures 1a and b depict a single cell for a MAC grid in the cartesian (x, y) and computational (ξ, η) planes, respectively.

We now follow geometric arguments given in [10] to develop relations needed for the discretization of Eqs. (1.1)–(1.3) in curvilinear coordinates. According to the chain rule, the ξ- and η-derivatives of ϕ are related to the x- and y-derivatives by

$$\phi_\xi = x_\xi \phi_x + y_\xi \phi_y \tag{2.1}$$

$$\phi_\eta = x_\eta \phi_x + y_\eta \phi_y. \tag{2.2}$$

Solving Eqs. (2.1) and (2.2) for ϕ_x and ϕ_y, we obtain

$$\phi_x = J^{-1}[y_\eta \phi_\xi - y_\xi \phi_\eta] \tag{2.3}$$

$$\phi_y = J^{-1}[x_\xi \phi_\eta - x_\eta \phi_\xi], \tag{2.4}$$

where J is the jacobian of the coordinate transformation,

$$J = x_\xi y_\eta - x_\eta y_\xi. \tag{2.5}$$

Since the grid has unit spacing in the computational plane, the length of a cell face of constant ξ is

$$S^{(\xi)} = \sqrt{x_\eta^2 + y_\eta^2} \tag{2.6}$$

and the length of a cell face of constant η is

$$S^{(\eta)} = \sqrt{x_\xi^2 + y_\xi^2}. \tag{2.7}$$

The unit vector normal to a face of constant ξ is

$$\mathbf{n}^{(\xi)} = \nabla\xi/|\nabla\xi| \tag{2.8}$$

and the unit vector normal to a face of constant η is

$$\mathbf{n}^{(\eta)} = \nabla\eta/|\nabla\eta|. \tag{2.9}$$

Substituting ξ and η for ϕ in Eqs. (2.3) and (2.4), we obtain

$$\xi_x = J^{-1} y_\eta \tag{2.10}$$

$$\xi_y = -J^{-1} x_\eta \tag{2.11}$$

$$\eta_x = -J^{-1} y_\xi \tag{2.12}$$

$$\eta_y = J^{-1} x_\xi. \tag{2.13}$$

The expressions given by Eqs. (2.10)–(2.13) are needed for the unit normal vectors, Eqs. (2.8) and (2.9).

3. CONSERVATION OF MASS

Assuming for convenience that $\rho = 1$, the mass flux through a given face (per unit depth) is the normal component of velocity multiplied by the length of the face. Thus, the mass flux through a face of constant ξ is

$$U = \mathbf{n}^{(\xi)} \cdot \mathbf{u} S^{(\xi)} \tag{3.1}$$

and the mass flux through a face of constant η is

$$V = \mathbf{n}^{(\eta)} \cdot \mathbf{u} S^{(\eta)}. \tag{3.2}$$

Combining Eqs. (2.6)–(2.13) with (3.1) and (3.2), we obtain expressions for the mass-flux components,

$$U = y_\eta u - x_\eta v \tag{3.3}$$

$$V = x_\xi v - y_\xi u, \tag{3.4}$$

where (u, v) are the cartesian components of the velocity.

A cell is defined by the cartesian coordinates $(\hat{x}, \hat{y})$ of its four corners (nodes). The normal components of mass flux through the east and north faces are then given by

$$U_e = \hat{y}^e_\eta u_e - \hat{x}^e_\eta v_e \tag{3.5}$$

$$V_n = \hat{x}^n_\xi v_n - \hat{y}^n_\xi u_n. \tag{3.6}$$

The subscripts and superscripts e, w, n, and s denote the east, west, north, and south faces, respectively. The hat ($\hat{}$) indicates that the ξ- and η-derivatives of the cartesian coordinates in Eqs. (3.5) and (3.6) are to be approximated with the difference equations,

$$\hat{x}^e_\eta = \hat{x}(i, j) - \hat{x}(i, j-1) \tag{3.7}$$

$$\hat{x}^n_\xi = \hat{x}(i, j) - \hat{x}(i-1, j) \tag{3.8}$$

with similar approximations for derivatives of $\hat{y}$.

The derivatives in Eqs. (3.5) and (3.6) are calculated with nodal (corner) coordinates, because these coordinates determine the lengths of the cell faces in Eqs. (2.6) and (2.7). Since Eqs. (3.7) and (3.8) each use only two corner nodes, we shall call them *two-node* approximations for the coordinate derivatives.

Mass is conserved for a given cell when its flux components satisfy the discrete analog of Eq. (1.2),

$$U_e - U_w + V_n - V_s = 0. \tag{3.9}$$

Suppose there exists a velocity (u', v') with corresponding mass flux (U', V') that does not satisfy (3.9). Adding the gradient of a scalar potential, we obtain

$$u = u' - \phi_x \tag{3.10}$$

$$v = v' - \phi_y. \tag{3.11}$$

After adjustment of (u', v') by Eqs. (3.10) and (3.11), the mass-flux components through the east and north faces become

$$U_e = U'_e - \alpha_e \phi^e_\xi + \gamma_e \phi^e_\eta \tag{3.12}$$

$$V_n = V'_n - \beta_n \phi^n_\eta + \gamma_n \phi^n_\xi, \tag{3.13}$$

where

$$\alpha_e = J_e^{-1}[\hat{x}^e_\eta x^e_\eta + \hat{y}^e_\eta y^e_\eta] \tag{3.14}$$

$$\beta_n = J_n^{-1}[\hat{x}^n_\xi x^n_\xi + \hat{y}^n_\xi y^n_\xi] \tag{3.15}$$

$$\gamma_e = J_e^{-1}[\hat{x}^e_\eta x^e_\xi + \hat{y}^e_\eta y^e_\xi] \tag{3.16}$$

$$\gamma_n = J_n^{-1}[\hat{x}^n_\xi x^n_\eta + \hat{y}^n_\xi y^n_\eta] \tag{3.17}$$

with similar expressions for the west and south faces. The Jacobian for the east face is

$$J_e = x^e_\xi y^e_\eta - x^e_\eta y^e_\xi \tag{3.18}$$

with similar expressions for the Jacobians on the north, west, and south faces. Note that the coefficients given by Eqs. (3.16) and (3.17) should be identically zero if the coordinates are orthogonal, and nonzero otherwise.

The coordinate derivatives with the hat ($\hat{}$) come from Eqs. (3.5) and (3.6), and they must be computed with the two-node approximations given by Eqs. (3.7) and (3.8).

Those without the hat come from Eqs. (2.3) and (2.4), and they may be computed by other means. Thus, distinct approximations are allowed for the coordinate derivatives in the gradient and the mass flux.

Substituting Eqs. (3.12) and (3.13) into (3.9), we obtain the discrete analog of the Poisson equation (1.3),

$$\alpha_e\phi^e_\xi - \gamma_e\phi^e_\eta - \alpha_w\phi^w_\xi + \gamma_w\phi^w_\eta + \beta_n\phi^n_\eta - \gamma_n\phi^n_\xi - \beta_s\phi^s_\eta + \gamma_s\phi^s_\xi = U'_e - U'_w + V'_n - V'_s. \quad (3.19)$$

When Eq. (3.19) is satisfied for every cell on the grid, then mass-conserving flux components can be obtained from Eqs. (3.12) and (3.13) for every cell face on the grid.

4. AMBIGUOUS COORDINATE DERIVATIVES

Following standard procedure for MAC grids, we place the discrete potential $\phi(i,j)$ at the center of the cell whose northeast corner is located at node (i,j) in the computational plane (Fig. 1b). Note that the integers (i,j) now serve as discrete curvilinear coordinates *and* as labels for cell (i,j), which is the cell under consideration.

We obtain cell-centered coordinates $(\bar{x}, \bar{y})$ for cell (i,j) by averaging the nodal coordinates,

$$\bar{x}(i,j) = \tfrac{1}{4}[\hat{x}(i,j) + \hat{x}(i-1,j) + \hat{x}(i,j-1) + \hat{x}(i-1,j-1)] \quad (4.1)$$

$$\bar{y}(i,j) = \tfrac{1}{4}[\hat{y}(i,j) + \hat{y}(i-1,j) + \hat{y}(i,j-1) + \hat{y}(i-1,j-1)]. \quad (4.2)$$

Given these definitions, the central-difference expressions for ξ-derivatives of ϕ, x, and y on the east face are the *two-cell* approximations,

$$\phi^e_\xi = \phi(i+1,j) - \phi(i,j) \quad (4.3)$$

$$x^e_\xi = \bar{x}(i+1,j) - \bar{x}(i,j) \quad (4.4)$$

$$y^e_\xi = \bar{y}(i+1,j) - \bar{y}(i,j). \quad (4.5)$$

Likewise, the central-difference expressions for η-derivatives of ϕ, x, and y on the north face are the *two-cell* approximations,

$$\phi^n_\eta = \phi(i,j+1) - \phi(i,j) \quad (4.6)$$

$$x^n_\eta = \bar{x}(i,j+1) - \bar{x}(i,j) \quad (4.7)$$

$$y^n_\eta = \bar{y}(i,j+1) - \bar{y}(i,j). \quad (4.8)$$

Since $\phi(i,j)$ is defined only at the cell centers, the central-difference expression for its η-derivative on the east face is the *four-cell* approximation,

$$\phi^e_\eta = \tfrac{1}{4}[\phi(i+1,j+1) - \phi(i+1,j-1) + \phi(i,j+1) - \phi(i,j-1)] \quad (4.9)$$

and the central-difference expression for its ξ-derivative on the north face is the *four-cell* approximation,

$$\phi^n_\xi = \tfrac{1}{4}[\phi(i+1,j+1) - \phi(i-1,j+1) + \phi(i+1,j) - \phi(i-1,j)]. \quad (4.10)$$

In contrast, the choices for similar derivatives of x and y are not so limited as those for ϕ. In fact, the simplest central-difference expressions for these derivatives are the *two-node* approximations given by Eqs. (3.7) and (3.8), e.g.,

$$x^e_\eta = \hat{x}(i,j) - \hat{x}(i,j-1) \quad (4.11)$$

$$x^n_\xi = \hat{x}(i,j) - \hat{x}(i-1,j). \quad (4.12)$$

As an alternative to Eqs. (4.11) and (4.12), we might consistently use identical approximations for derivatives of x, y, and ϕ that occur in the gradient. In that case, Eqs. (4.11) and (4.12) would be superseded by

$$x^e_\eta = \tfrac{1}{4}[\bar{x}(i+1,j+1) - \bar{x}(i+1,j-1) + \bar{x}(i,j+1) - \bar{x}(i,j-1)] \quad (4.13)$$

$$x^n_\xi = \tfrac{1}{4}[\bar{x}(i+1,j+1) - \bar{x}(i-1,j+1) + \bar{x}(i+1,j) - \bar{x}(i-1,j)]. \quad (4.14)$$

We shall call x^e_η, y^e_η, x^n_ξ, and y^n_ξ *ambiguous* coordinate derivatives, because it is not yet clear whether to use Eqs. (4.11) and (4.12), or (4.13) and (4.14), for their discrete representation in the gradient.

5. AMBIGUOUS PRESSURE DERIVATIVES

Suppose that the east face of a given cell lies on a boundary (Fig. 2) for which no correction is needed in the normal component of mass flux, i.e.,

$$U_e = U'_e. \quad (5.1)$$

This imposes a Neumann condition on the flux of the gradient through the boundary, such that

$$\alpha_e\phi^e_\xi - \gamma_e\phi^e_\eta = 0. \quad (5.2)$$

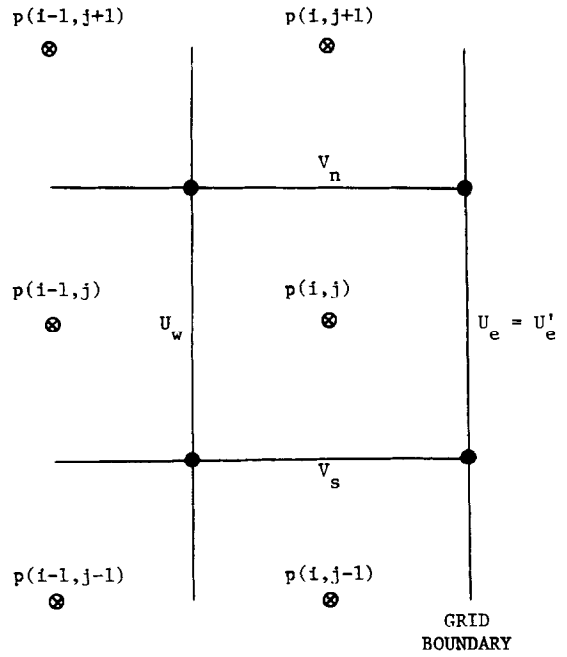

FIG. 2. Grid cell (i, j) with east face lying entirely on a boundary in the computational plane.

If we substitute Eq. (5.2) into (3.19), the discrete Poisson equation reduces to

$$-\alpha_w\phi^w_\xi+\gamma_w\phi^w_\eta+\beta_n\phi^n_\eta-\gamma_n\phi^n_\xi-\beta_s\phi^s_\eta+\gamma_s\phi^s_\xi = U'_e-U'_w+V'_n-V'_s. \tag{5.3}$$

Note that Eq. (5.3) does not include derivatives of ϕ on the east face, which coincides with the boundary; but it does include derivatives on the north and south faces, which terminate on the boundary. In this case the η-derivative presents no problem on the north or south face, because the η-direction is tangent to the boundary. The η-derivative can be approximated on these faces with Eq. (4.6), which uses only ϕ-values inside the grid.

In contrast, the ξ-direction here is the off-boundary direction. If Eq. (4.10) is used for the ξ-derivative on the north face, then ϕ-values are needed outside the grid in cells $(i+1, j)$ and $(i+1, j+1)$. Likewise, the ξ-derivative on the south face requires ϕ-values in cells $(i+1, j)$ and $(i+1, j-1)$. Since it is not yet clear how to provide the needed values of ϕ in these derivatives, we shall call them *ambiguous* derivatives of ϕ on the north and south faces.

In this situation we have at least two alternatives. First, we might assume that the relation between ξ- and η-derivatives on the east face also holds on the north and south faces. Thus, we might use Neumann conditions, similar to Eq. (5.2), to calculate ϕ_ξ from ϕ_η on the north and south faces, e.g.,

$$\phi^n_\xi=\frac{\gamma_n}{\alpha_n}\phi^n_\eta. \tag{5.4}$$

We shall call Eq. (5.4) the *Neumann* approximation for the ambiguous derivative of ϕ, with which the discrete Poisson equation (5.3) reduces to

$$-\alpha_w\phi^w_\xi+\gamma_w\phi^w_\eta+\beta'_n\phi^n_\eta-\beta'_s\phi^s_\eta = U'_e-U'_w+V'_n-V'_s, \tag{5.5}$$

where

$$\beta'_n=\beta_n-\gamma_n^2/\alpha_n \tag{5.6}$$

with a similar expression for β'_s. This eliminates the ambiguous ξ-derivatives, and likewise the need for Eq. (4.10), on the north and south faces.

As a second alternative, we might use linear extrapolation to calculate ϕ-values outside the boundaries from ϕ-values inside the grid, and then substitute the extrapolated ϕ-values into Eq. (4.10); e.g.,

$$\phi(i+1,j)=2\phi(i,j)-\phi(i-1,j) \tag{5.7}$$

$$\phi(i+1,j+1)=2\phi(i,j+1)-\phi(i-1,j+1), \tag{5.8}$$

in which case Eq. (4.10) reduces to the one-sided four-cell approximation,

$$\phi^n_\xi=\tfrac{1}{2}[\phi(i,j+1)-\phi(i-1,j+1)+\phi(i,j)-\phi(i-1,j)]. \tag{5.9}$$

For future reference, we shall call Eq. (5.9) the *one-sided* approximation for the ambiguous derivative of ϕ.

In general, if the east face or the west face lies on a boundary, the ξ-derivatives of ϕ are ambiguous on the north and south faces.

Likewise, if the north face or the south face lies on a boundary, the η-derivatives of ϕ are ambiguous on the east and west faces. For example, if the north face lies on a boundary, the Neumann approximation for the η-derivative of ϕ on the east face is

$$\phi^e_\eta=\frac{\gamma_e}{\beta_e}\phi^e_\xi \tag{5.10}$$

and the one-sided approximation for the same derivative is

$$\phi^e_\eta=\tfrac{1}{2}[\phi(i+1,j)-\phi(i+1,j-1)+\phi(i,j)-\phi(i,j-1)]. \tag{5.11}$$

A third alternative is to average the one-sided and Neumann approximations. This was investigated in [1], where it proved superior to the simple Neumann approximation, but inferior to the purely one-sided approximation. Other possibilities include the use of higher-order approximations for the ambiguous derivatives, but these complicate the discrete laplacian in boundary-adjacent cells. For the sake of brevity and simplicity, we consider only the Neumann and one-sided approximations here.

6. DISCRETE SOLUTION

Let us now summarize the discretization procedure for any given cell. In the mass-flux components given by Eqs. (3.3) and (3.4), we use two-node approximations, as defined by Eqs. (3.7) and (3.8), for η-derivatives of x and y on the east and west faces, and also for ξ-derivatives of x and y on the north and south faces.

Otherwise, in the components of the gradient given by Eqs. (2.3) and (2.4), we use two-cell approximations, as defined by Eqs. (4.3)–(4.5), for ξ-derivatives of x, y, and ϕ on the east and west cell faces; and also, as defined by Eqs. (4.6)–(4.8), for η-derivatives of x, y, and ϕ on the north and south faces.

On the east and west faces, we have proposed two alternatives for the (ambiguous) η-derivatives of x and y in the gradient. That is, we can use either the two-node approximation given by Eq. (4.11), or the four-cell approximation given by Eq. (4.13). On the north and south faces, we have similar alternatives for the (ambiguous) ξ-derivatives of x and y in the gradient. Note that whenever a four-cell approximation requires values of $\bar{x}$ and $\bar{y}$ outside the grid, we can supply these by linear extrapolation.

For cells that do not touch any boundary, we can always use two-cell approximations for ξ-derivatives of ϕ on the east and west faces, and likewise for η-derivatives of ϕ on the north and south faces. In the same situation, we can always use four-cell approximations for η-derivatives of ϕ on east and west faces, and likewise for ξ-derivatives of ϕ on north and south faces.

When an entire face lies on a boundary, we impose a zero-flux (Neumann) condition, e.g., Eq. (5.2), for the gradient of ϕ. This eliminates the need for approximating derivatives of ϕ on the boundary itself, but it still leaves one ambiguous derivative for each face that terminates on the boundary. Here again we have proposed two alternatives for the ambiguous derivatives. We can use the Neumann approximation, e.g., Eq. (5.4), in which we obtain the ambiguous derivative from the other (unambiguous) derivative via the Neumann condition. Or we can use linear extrapolation of ϕ across the boundary to derive a one-sided approximation, e.g., Eq. (5.9), for the ambiguous derivative. Note that the second alternative applies only for cell faces that terminate on a boundary; it does not alter the Neumann condition for a cell face that lies entirely on a boundary.

The procedures we have outlined cover all possibilities except those in which a corner (node) lies on a boundary, but in which no entire face lies on a boundary. In such cases, we still exercise the same alternatives for ambiguous derivatives of ϕ in the off-boundary direction.

When the difference approximations for the derivatives of ϕ are inserted in the left-hand side of Eq. (3.19), there results a discrete Poisson equation that relates $\phi(i, j)$ to the values in the eight cells immediately surrounding cell (i, j). Each grid cell contributes one equation of this kind to a set of linear equations for the grid as a whole. To solve these equations for $\phi(i, j)$, we use the (iterative) preconditioned conjugate-gradient scheme reported by Kapitza and Eppel [4].

Having obtained the discrete solution for ϕ, we can calculate the mass-conserving flux components from Eqs. (3.12) and (3.13). Here it is important to use the same coefficients and the same approximations for the ξ- and η-derivatives of ϕ that were used in Eq. (3.19). Otherwise, the computed flux components will not satisfy Eq. (3.9), in which case they will not conserve mass.

7. TEST PROBLEMS

To test the proposed alternatives for discretization, we have chosen two straight channels in the cartesian (x, y)

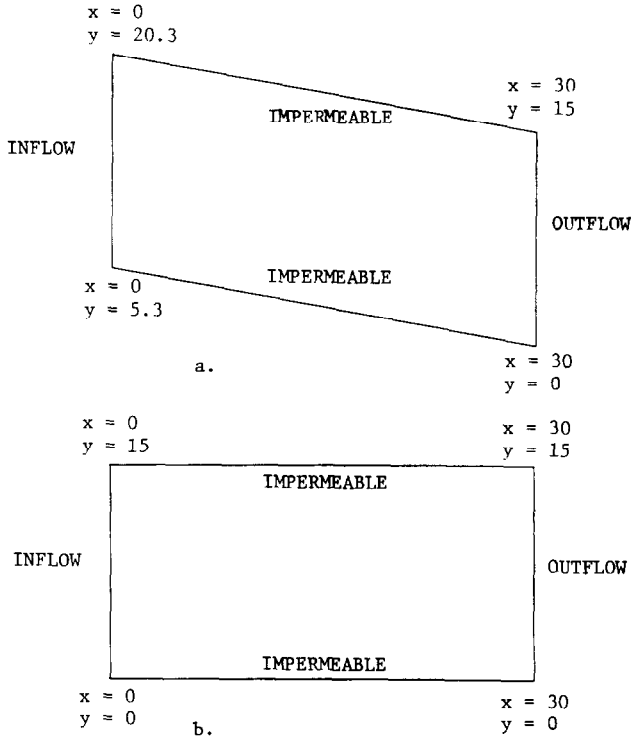

FIG. 3. Orientation of test channels in the cartesian plane: (a) slanted channel; (b) horizontal channel.

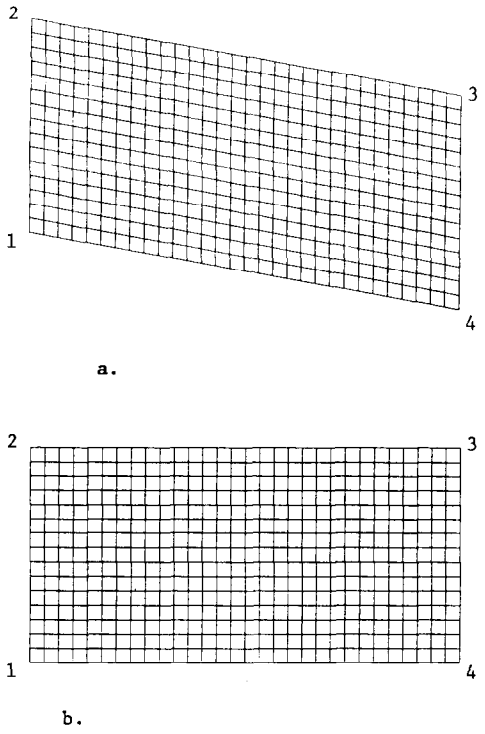

FIG. 4. Computational grid for slanted channels: (a) cartesian (x, y) plane; (b) computational (ξ, η) plane.

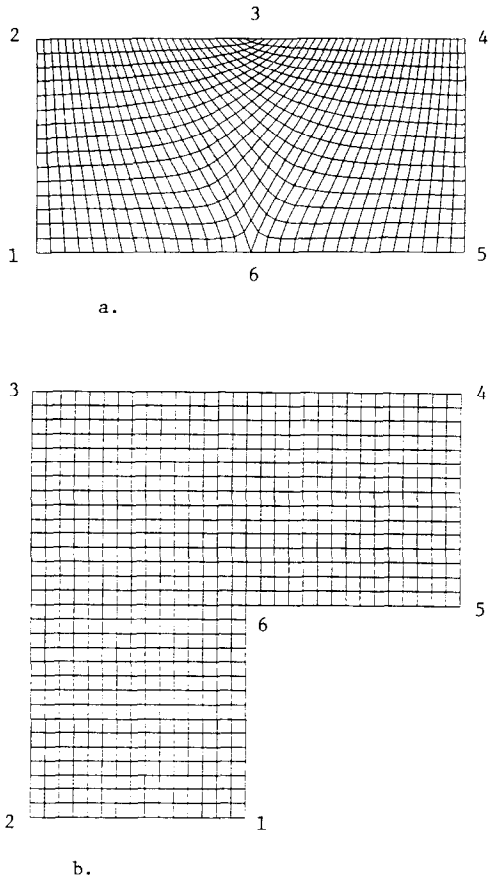

FIG. 5. Computational grid for horizontal channels: (a) cartesian (x, y) plane; (b) computational (ξ, η) plane.

plane (Fig. 3). The first channel is slanted downward by 10°, and the second is perfectly horizontal. In each case, flow enters through the left boundary ($x = 0$) and exits through the right boundary ($x = 30$). The upper and lower boundaries are impermeable, and they are separated by a y-distance of 15 in both channels.

To impose a test flow that is initially free of vorticity, but which does not conserve mass, we set $u' = 1$ and $v' > 0$ in both channels. This creates continuity violations at the upper and lower boundaries, but these can be corrected via Eq. (1.1) to make the flow mass-conserving everywhere.

The slanted channel has been fitted with a uniform, nonorthogonal grid in the cartesian (x, y) plane (Fig. 4a), which maps into a rectangle in the computational (ξ, η) plane (Fig. 4b). This grid allows the effects of nonorthogonality to be tested without the added complication of nonuniformity.

The horizontal channel has been fitted with a nonuniform, nonorthogonal grid (Fig. 5a), generated numerically with a code developed by Thompson [9]. Note that the channel boundaries are rectangular in the cartesian (x, y) plane (Fig. 5a), but they make an inverted L-shape in the computational (ξ, η) plane (Fig. 5b).

By using distorted grids with flows that should be uniform, we can test alternative discretization procedures in situations where deviations from the exact solutions will be easy to recognize. One convenient way to see departures from uniform flow is to examine the streamlines for the computed mass-conserving flow. These are curves along which the stream function ψ is constant, where ψ is related to the mass-flux components by

$$\psi_\eta = U \tag{7.1}$$

$$\psi_\xi = -V. \tag{7.2}$$

The stream function can easily be found by numerical integration of either Eq. (7.1) or Eq. (7.2). Since the grids have unit spacing in the computational (ξ, η) plane, the η-integral of U is merely a sum over the j-index, and the ξ-integral of V is a sum over the i-index.

The computed streamlines for the test problems should be perfectly straight in the cartesian (x, y) plane. Any deviation from this condition indicates that vorticity has been introduced into the flow by the discrete gradient of ϕ.

8. COMPUTED RESULTS

We now present streamlines computed for the two channels with different combinations of alternatives for the discrete gradient:

a. Nonorthogonal terms omitted ($\gamma \equiv 0$), with two-node approximations for the remaining ambiguous derivatives of x and y in α and β.

b. Nonorthogonal terms retained, with two-node approximations for ambiguous derivatives of x and y throughout the flow, and Neumann approximations for ambiguous derivatives of ϕ next to the boundaries.

c. Nonorthogonal terms retained, with two-node approximations for ambiguous derivatives of x and y throughout the flow, and one-sided approximations for ambiguous derivatives of ϕ next to the boundaries.

d. Nonorthogonal terms retained, with identical two-cell and four-cell approximations for derivatives of x, y, and ϕ throughout the flow, and one-sided approximations for ambiguous derivatives next to the boundaries.

Calculations have been done for both of the channels and each of the four combinations of alternatives, with $u' = 1$ and $v' > 0$. In each case, results have been obtained for

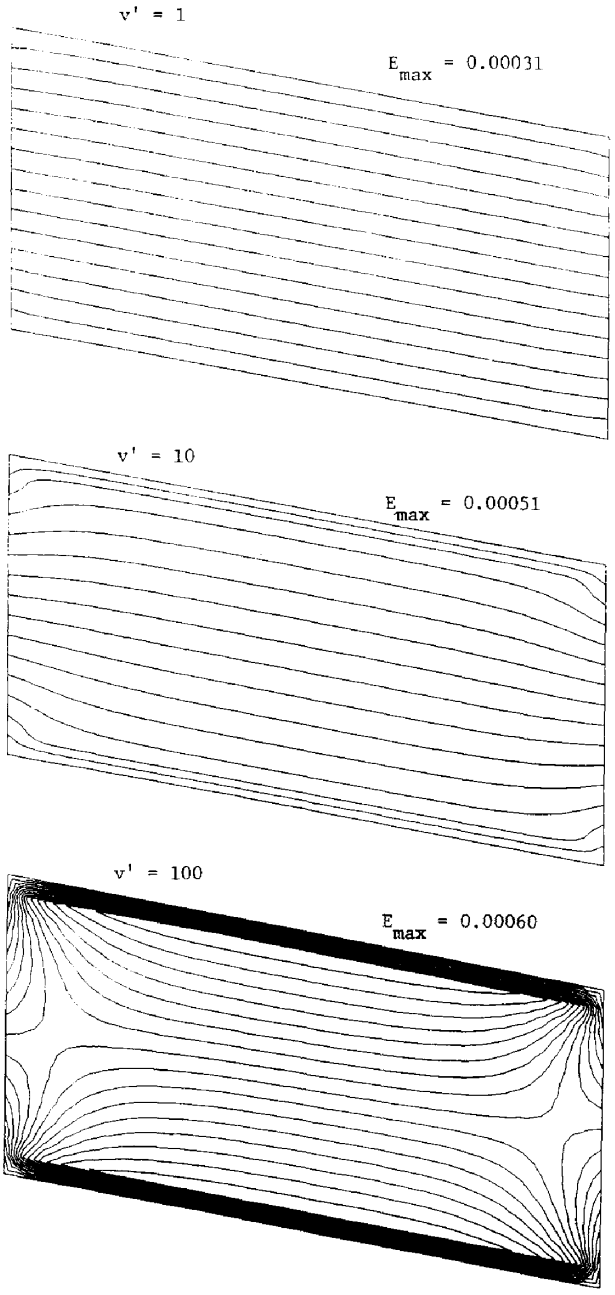

FIG. 6. Computed streamlines for slanted channel: Neumann approximation for ambiguous pressure derivatives next to boundaries.

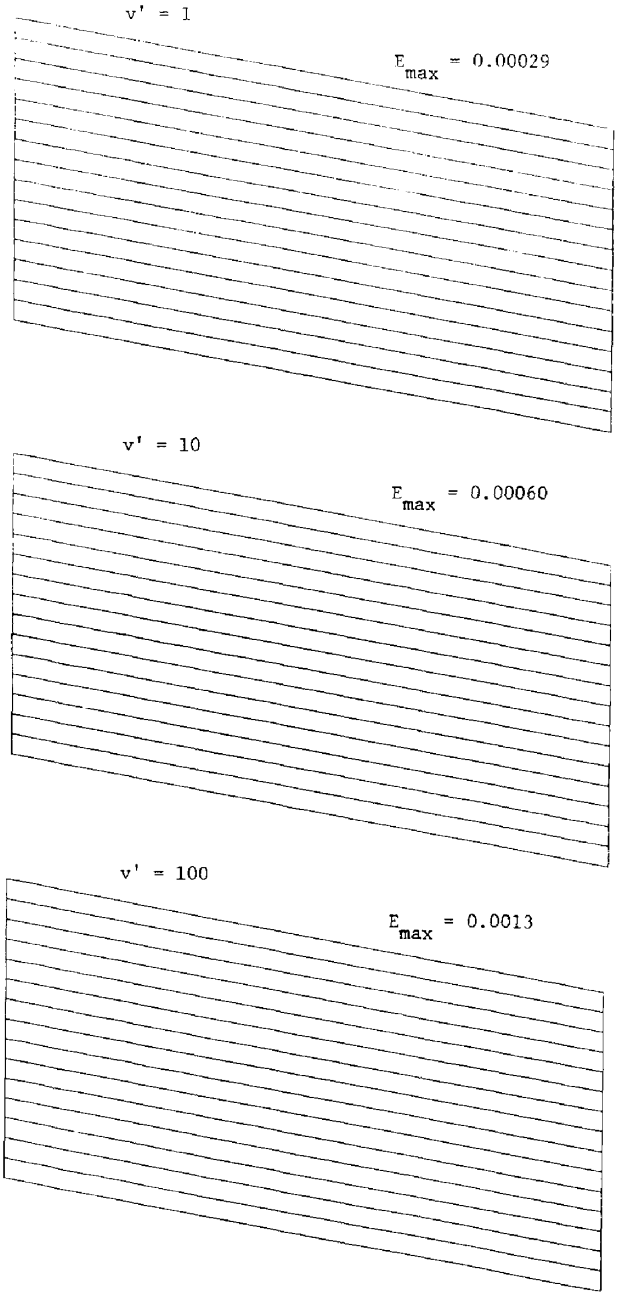

FIG. 7. Computed streamlines for slanted channel: One-sided approximation for ambiguous pressure derivatives next to boundaries.

$v' = 1$, $v' = 10$, and $v' = 100$. Computed streamlines are shown for the slanted channel in Figs. 6 and 7, and for the horizontal channel in Figs. 8–11.

For each cell, the relative mass-flux imbalance E is defined to be

$$E = \frac{2\,|U_e - U_w + V_n - V_s|}{|U_e| + |U_w| + |V_n| + |V_s|}. \tag{8.1}$$

This is the difference between the rates of mass inflow and mass outflow, divided by the average mass-flow rate through the cell faces. Thus, it represents the residual relative error in the continuity equation. Trial calculations (unpublished) have demonstrated that further changes in the plotted streamlines become indiscernible when the maximum residual $E_{\max}$ is 0.01 or less.

Sixty iterations were used for the conjugate-gradient Poisson solver in each flow calculation. (For programming reasons this was more convenient than iterating to a prespecified error tolerance.) In the *worst* case (Fig. 10), the maximum residual was $E_{\max} = 0.0044$. In Figs. 6–11, each set of plotted streamlines is labeled with the starting value of v' and the final value of $E_{\max}$. The contour interval for the streamlines is $\Delta\psi = 1$.

The results for discrete combination b in the slanted channel (Fig. 6) make it clear that the Neumann approximation

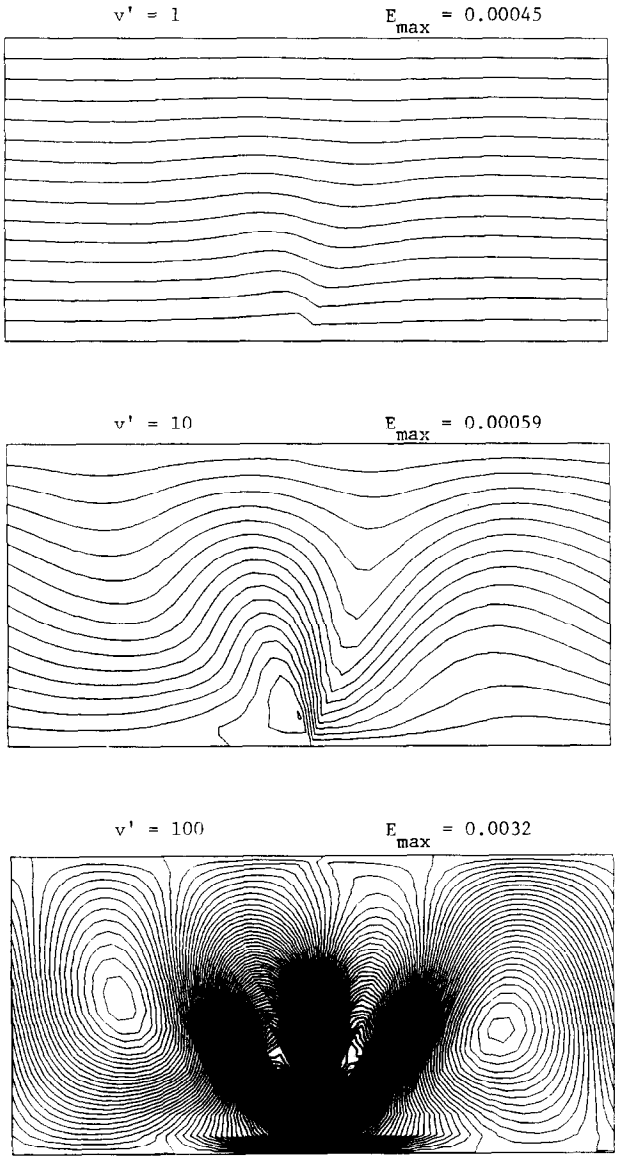

FIG. 8. Computed streamlines for horizontal channel: Non-orthogonal terms omitted from discrete gradient altogether.

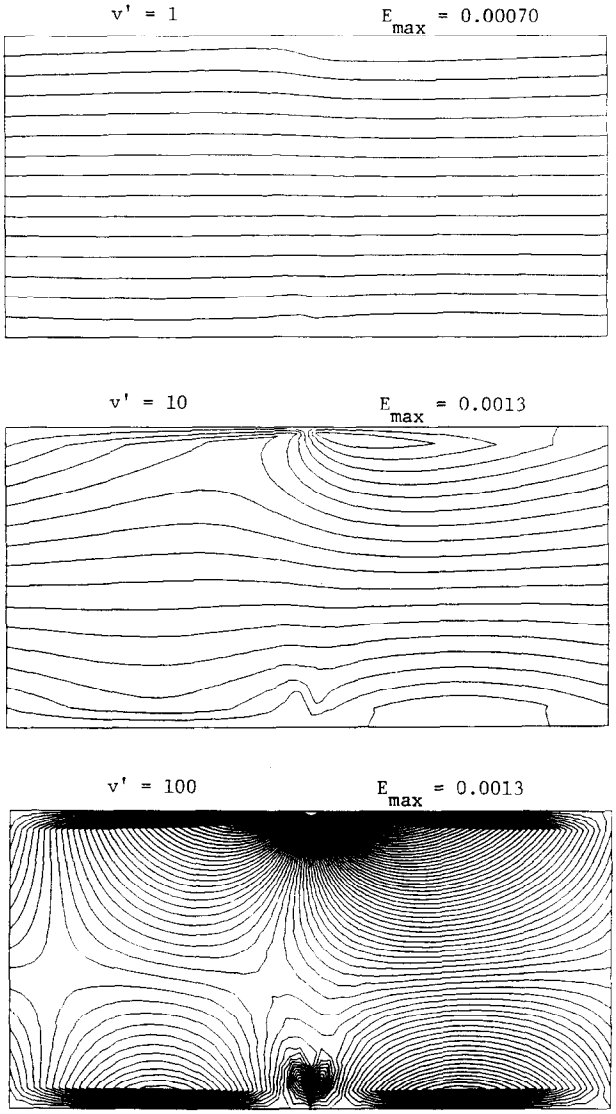

FIG. 9. Computed streamlines for horizontal channel: Neumann approximation for ambiguous pressure derivatives next to boundaries, and two-node approximation for ambiguous coordinate derivatives throughout the flow.

is unsuitable for ambiguous derivatives of ϕ even when the grid is uniform. In this case the ambiguous derivatives of x and y are the same whether we use two-node approximations or four-cell approximations, because all derivatives of x and y are constant for the entire grid.

The plotted streamlines are indistinguishable for discrete combinations a, c, and d in the slanted channel, and only those for combination c are shown in Fig. 7. Here one might surmise that it is equally admissible either to keep the nonorthogonal terms and use one-sided approximations for ambiguous derivatives of ϕ next to the boundaries, or to drop the nonorthogonal terms from the discrete gradient altogether. This would be premature, however, because Fig. 7 illustrates none of the effects of grid nonuniformity.

The distorted grid for the horizontal channel (Fig. 5a) imposes the coupled influences of nonorthogonality and nonuniformity, and Fig. 8 shows the streamlines obtained for this case with discrete combination a. The figure leaves little doubt about the folly of dropping nonorthogonal terms from the discrete pressure gradient for general curvilinear MAC grids.

In Fig. 9, the streamlines plotted for discrete combination b offer further evidence that the Neumann approximation is unsuitable for ambiguous pressure derivatives. And although combination c offers marked improvement over combination b, it is evident from Fig. 10 that the one-sided approximation for ambiguous pressure derivatives still leads to spurious vorticity when used with two-node approximations for ambiguous coordinate derivatives.

Only discrete combination d achieves conservation of

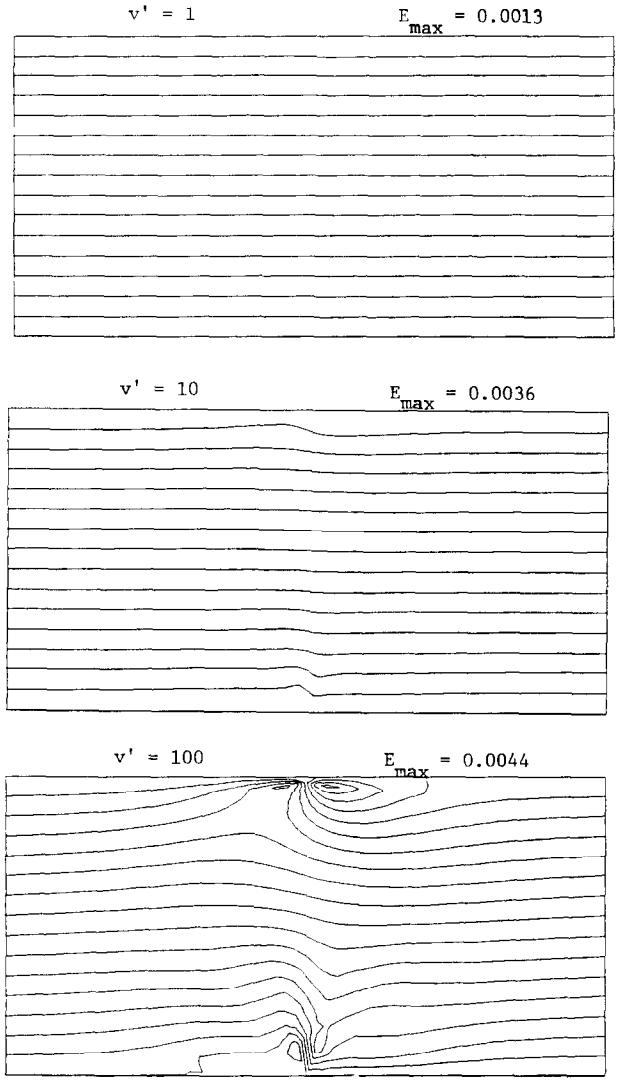

FIG. 10. Computed streamlines for horizontal channel: One-sided approximation for ambiguous pressure derivatives next to boundaries, and two-node approximation for ambiguous coordinate derivatives throughout the flow.

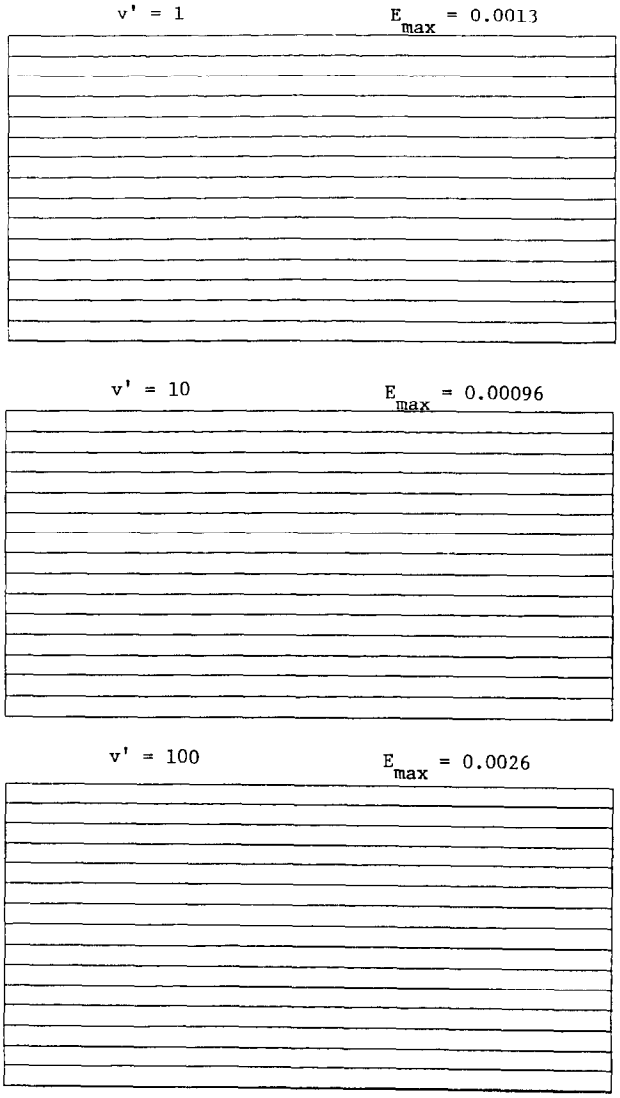

FIG. 11. Computed streamlines for horizontal channel: Identical approximations for pressure derivatives and coordinate derivatives throughout the flow, with one-sided approximations for ambiguous derivatives next to boundaries.

mass without adding vorticity to the flow, as indicated by the computed streamlines in Fig. 11. This demonstrates the effect of using identical approximations for coordinate derivatives and pressure derivatives throughout the flow, with one-sided approximations for ambiguous derivatives next to the boundaries.

9. CONCLUSION

By trial and error with nonorthogonal MAC grids, we have arrived at guidelines for discretizing the cartesian components of the pressure gradient given by Eqs. (2.3) and (2.4). First, all terms arising from nonuniformity and nonorthogonality should be retained. Second, pressure derivatives and coordinate derivatives should be represented with identical finite-difference approximations. Third, ambiguous derivatives next to boundaries should be represented with one-sided approximations in the off-boundary direction.

In order to achieve identical approximations for coordinate derivatives and pressure derivatives in Eqs. (2.3) and (2.4), it is necessary that coordinate values and pressure values be taken from the same discrete locations (the cell centers in this case). The exclusive use of cell-centered coordinates or nodal coordinates guarantees that the difference approximations for $x_{\xi\eta}$ and $x_{\eta\xi}$ will be identical, but the mixed use of nodal and cell-centered coordinates does not. It is important that the cross derivatives of x and y commute for reasons that become apparent only with hindsight.

Recall that Eqs. (2.3) and (2.4) were obtained simply by imposing the chain rule for derivatives. A more rigorous derivation for finite-volume applications might begin with the Gauss divergence theorem, which leads to the expressions [10]:

$$\phi_x = J^{-1}[(y_\eta \phi)_\xi - (y_\xi \phi)_\eta] \tag{9.1}$$

$$\phi_y = J^{-1}[(x_\xi \phi)_\eta - (x_\eta \phi)_\xi]. \tag{9.2}$$

Equations (2.3) and (2.4) are equivalent to (9.1) and (9.2) only if the identities $x_{\xi\eta} = x_{\eta\xi}$ and $y_{\xi\eta} = y_{\eta\xi}$ are satisfied. Failure to meet this criterion apparently gives rise to the distorted streamlines in Fig. 10, which were obtained by using nodal coordinates with cell-centered pressures in Eqs. (2.3) and (2.4). From this we surmise that cell-centered coordinates should be used exclusively with cell-centered pressures to approximate the derivatives in the gradient for MAC grids. Note, however, that nodal coordinates should still be used to compute flux normal to the cell faces, as in Eqs. (3.5) and (3.6).

The failure of the Neumann approximation, and the success of the one-sided approximation, for ambiguous pressure derivatives next to the boundaries may seem counter-intuitive, but it is easily explained in retrospect. In order to eliminate a large continuity violation in a boundary-adjacent cell, the discrete Poisson equation requires a proportionately large difference between the normal pressure derivative on the boundary-coincident face and the corresponding derivatives on the other three faces. This makes the Neumann condition (zero normal derivative) a poor approximation for conditions anywhere except the boundary itself. For cell faces that terminate on the boundary, the one-sided approximation is a much better (first-order) approximation for derivatives in the off-boundary direction, because it places no constraint on these derivatives in advance. In short, the Neumann condition turns out to be more important for constraining the flux of the gradient *through* the boundaries than for determining the steepness of the gradient *near* the boundaries.

The guidelines established here for pressure discretization are important for general curvilinear MAC grids, regardless of the particular technique used to solve the incompressible Euler or Navier–Stokes equations. Moreover, the same rules apply whether the pressure is computed by using artificial compressibility [7], or by solving a Poisson equation. The important thing is that derivatives be approximated in such a way that the pressure gradient achieves conservation of mass without adding vorticity to the flow.

ACKNOWLEDGMENT

This paper was prepared under Work Unit 32319 of the Repair, Evaluation, Maintenance, and Rehabilitation Research Program of the U.S. Army Corps of Engineers. Permission to publish was granted by Headquarters, U.S. Army Corps of Engineers.

REFERENCES

1. R. S. Bernard, in *Transactions of the Fifth Army Conference on Applied Mathematics and Computing, 1987* (ARO Report 88-1, U.S. Army Research Office), pp. 631–641.
2. J. H. Ferziger, *J. Comput. Phys.* **69**, 1 (1987).
3. F. H. Farlow and J. E. Welch, *Phys. Fluids* **8**, 2182 (1965).
4. H. Kapitza and D. Eppel, *J. Comput. Phys.* **68**, 474 (1987).
5. F. Mesinger and A. Arakawa, "Numerical Methods Used in Atmospheric Models, Vol. 1," GARP Publ. Ser., No. 17 (Unpub., New York, 1976), p. 64.
6. S. V. Patankar, *Numerical Heat Transfer and Fluid Flow* (McGraw–Hill, New York, 1980).
7. R. Peyret and T. D. Taylor, *Computational Methods for Fluid Flow* (Springer-Verlag, New York, 1983).
8. P. J. Roache, *Computational Fluid Dynamics* (Hermosa, Albuquerque, NM, 1976).
9. J. F. Thompson, Technical Report E-83-8, U.S. Army Engineer Waterways Experiment Station, Vicksburg, MS (unpublished).
10. J. F. Thompson, Z. U. A. Warsi, and C. W. Mastin, *Numerical Grid Generation: Foundations and Applications* (North-Holland, New York, 1985), pp. 120–147.